Development of Functional Near-infrared Spectroscopy Analysis Methods to Support Biomarker Investigation for Disordered Children

理工学研究科博士課程後期課程　都市人間環境学専攻 ストコ　ステファニー　リアナ　ウタミ
Graduate School of Science and Engineering, Civil, Human and Environmental Science and Engineering Course
Stephanie Liana Utami SUTOKO

I. Introduction

The prevalence of any developmental disorders increased from 12.84% to 16.2–17.8% in 20 years (1997–2017).[1,2] Among developmental disorders, attention-deficit/hyperactivity disorder (ADHD) has the highest prevalence rate with an increasing trend.[3] ADHD is commonly diagnosed based on the behavioral assessment using standard guidelines, such as the Diagnostic and Statistical Manual of Mental Disorders (DSM) and the International Classification of Diseases (ICD). However, diagnostic results using two standard guidelines showed discrepancies.[4,5] Another perspective of biomarker is sought out to diagnose ADHD.

ADHD is characterized by age-inappropriate inattention and/or hyperactivity/impulsivity. Controlling executive functions and behaviors has been well known as one of brain functions. Thus, measuring brain functions may be promising approaches for biomarkers.[6,7] There are several intervention-free modalities. However, from the perspectives of measurement convenience, spatial-temporal resolution, and efficiency, functional near-infrared spectroscopy (fNIRS) is considerably an optimum technique to perform pediatric studies. fNIRS measures cerebral hemodynamic changes [oxygenated (O_2Hb) and deoxygenated (HHb) hemoglobin] that are closely connected to the brain activity.[8]

fNIRS was developed for more than 25 years ago,[9] and it has also been applied to many fields, such as neurology, psychiatry, psychology, and basic research.[10] ADHD studies have also been pursued using fNIRS in evaluating disorder characteristics and monitoring medication effects.[11-14] Those applications should be supported by reliable analysis methods. Analysis purposes are categorized in removing noises (endogenous[15-18] and exogenous[19,20]) and extracting brain function information.[21-23] ADHD children measurement encounters the heightened risk of motion artifacts. Therefore, the development of analysis methods which are also able to remove motion artifacts are indispensable.

II. Scope of work

The objectives of this dissertation are to develop fNIRS analysis methods for disordered children measurement and to evaluate the applications of those methods on seeking ADHD biomarkers. These objectives are formulated in three frameworks (III–V).

First, the development of noise removal method to improve the conventional brain activation analysis (i.e., averages of signal amplitude during stimuli) and its application as a preprocessing step for a study of differential diagnostic biomarker. fNIRS measurements (Figure 1) are commonly carried out during performances of cognitive tasks [e.g., go/no-go (GNG), oddball (OB); Figure 2]. Cognitive tasks are designed following the block-design paradigm with alternating orders for baseline (BS) and stimulus. An epoch is defined as a span consisting of pre-stimulus (part of BS), stimulus, and post-stimulus (part of BS) intervals. Noisy epochs are conventionally rejected or corrected. Straightforward rejection through visual judgments will reduce statistical power ($1–\beta$); corrective methods may lead to overcorrection issues. Therefore, a method to reject noisy epochs by considering the trade-off between remaining noises and required statistical power was approached. This method was then applied on a measurement dataset of ADHD and autism spectrum disorder (ASD) comorbid ADHD children (i.e., disordered children). The noise-free data was analyzed to figure out the optimum biomarker for differentiating ASD-comorbid ADHD children from ADHD children.

Second, the development of static functional connectivity (FC) analysis method for the block-design paradigm and the comparisons between activation and static FC features for ADHD screening biomarkers. In order to improve the robustness, averanging noise-free

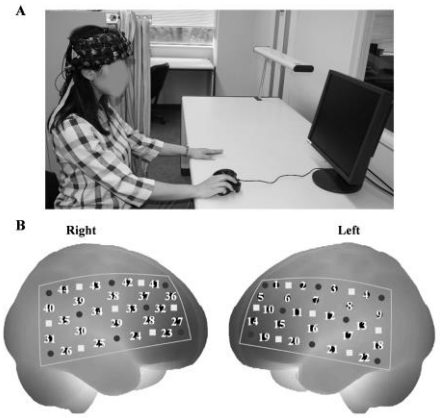

Figure 1. (A) Exemplary fNIRS measurement setup and (B) probe configuration (circles, squares, and numbered circles for emitter, detector, and channels, respectively). From [34], adapted with permission.

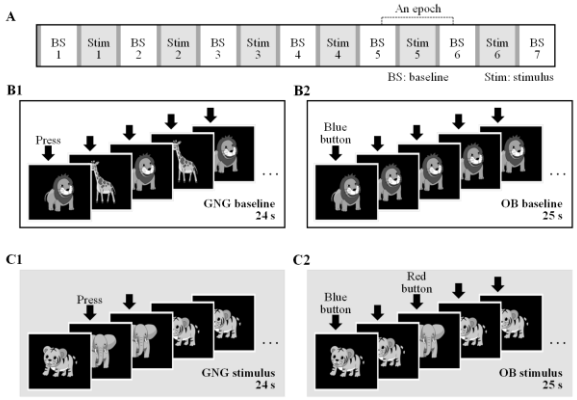

Figure 2. Task design. (A) The block-design paradigm with 3-s instructions in between baseline and stimulus. Specific commands for baseline (B) and stimulus (C) intervals for the GNG (B1, C1) and OB (B2, C2) tasks. From [32], modified with permission.

epochs is done for the activation analysis. However, this way is improper for the FC analysis due to the disorganized temporal information. Thus, instead of noisy epochs, the rejection was performed on noise-affected datapoints. The remaining channel-wise datapoints were correlated to each other to quantify static FCs. A process to specifically analyze BS and stimulus FCs was also developed. Differences between typically developing (TD) and disordered children were evaluated in BS and stimulus FCs. The activation analysis was also conducted in the same dataset. Both activation and static FCs features were optimized to classify disordered children from TD children.

Third, the development of dynamic FC analysis method for the block-design paradigm and its insights into ADHD characteristics. The stationary assumption is dismissed; the dynamic concept was introduced as several connectivity states were found to alternate across the temporal course.[24] The elimination of noisy datapoints is inappropriate because the dynamic FC analysis requires uninterrupted datapoints. Another analysis procedure was developed to support the dynamic FC analysis for children measurement data with noise risks. Channel-wise datapoints within a short temporal window were correlated to each other, and the temporal window was shifted across the entire measurement to quantify dynamic FCs. Altered connectivity states were hypothesized to be different for TD and ADHD children. The findings would be new insights into ADHD pathophysiology.

III. Adaptive rejection algorithm and its application for a preprocessing step

The developed method named as the adaptive rejection algorithm consisted of two processes – noise identification and rejection judgment. In the process of noise identification, three noise criteria were set, including spikes with recovery failure, baseline shifts, and high inter-epoch variabilities. Spikes occur due to motion artifacts; baseline shifts are commonly caused by recovery failure of motion artifacts and/or the physiological noises.[25-27] Noise-affected epochs show dissimilarities compared to noise-free epochs; noisy epochs result in high variabilities.

For the process of rejection judgment, the rejection rate (i.e., the number of rejected epochs) was initially determined. Each criterion was then examined in order. If the identified noisy epochs were more than the acceptable rejection, the rejection was halted. Otherwise, the rejection was executed. The jugdment was continued using other criteria on the remaining/non-rejected epochs. After all criteria has been evaluated, the rejection was done based on how many times epochs were saved from rejections if the remaining epochs was more than the rejection rate.

The adaptive rejection algorithm was confirmed in the synthetic and real datasets. By applying this algorithm, the hemodynamic response function (HRF) was recovered from the noisy synthetic dataset (Figure 3). The real datasets had been previously analyzed and reported;[13,14] the algorithm application on those datasets rejected noisy epochs reproducing all statistical inferences. Previous analyses adapted the visual judgement to identify noisy epochs. Performances of the adaptive rejection algorithm showed similar rejections (69.2–77.0%), activation signals ($r > 0.7$) and values ($\rho > 0.69$) compared to performances of the visual judgment. Through a simulation, it was

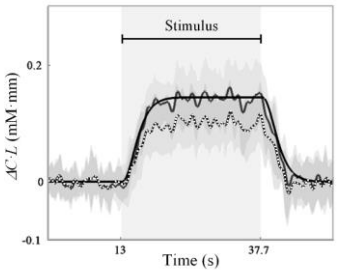

Figure 3. HRF recovery from the noisy synthetic dataset. The smooth plot is the ground truth; fluctuated solid and dotted lines are results of the adaptive rejection algorithm (β = 0.18) and no rejection (β = 0.34), respectively. Patches around plots indicate standard deviations. The temporal interval represents the epoch interval. From [32], adapted with permission.

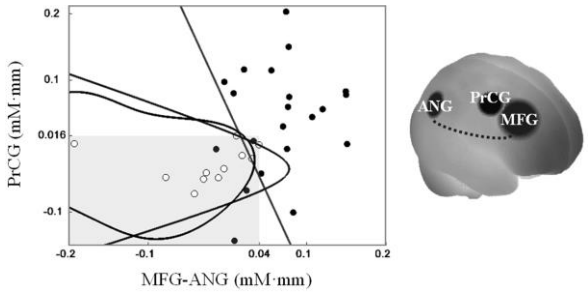

Figure 4. Medicated-evoked activations of the right PrCG against the MFG-ANG for ADHD (black bullets) and ASD-comorbid ADHD (white bullets) children.The shaded area and lines represent the most optimum differentiations using the OR operation [high MFG-ANG (attention function) ∨ high PrCG (motor function) for ADHD], linear and quadratic discriminants, and support vector machine. From [33], modified with permission.

confirmed that rejecting data still brought an adequate statistical power (> 0.8) as long as the activation phenomenon was profound.

The adaptive rejection algorithm was then applied on a different dataset[28] for a preprocessing step. The activation analysis was performed on noise-free epochs. Performances of ADHD and ASD-comorbid ADHD children were equal during the task (two-sample *t*-test, $p > 0.05$). However, their brain activation were distinct in the conditions of naïve and medicated (two-sample *t*-test, $p < 0.05$). Thus, brain-related characteristics were more significant than the behavioral-related ones; activation values were treated as promising biomarkers to support differential diagnosis. After an exhaustive optimization, activations in the right middle frontal (MFG), angular (ANG), and precentral (PrCG) gyri under the medicated condition [methylphenidate (MPH)] were found to be optimum biomarkers (82 ± 1.6% cross-validated accuracy). ADHD children showed higher activations in those regions than ASD-comorbid ADHD children (Figure 4). The appropriate preprocessing method is requisite to obtain robust and well-performed biomarkers; the current findings indicated the successful application of the adaptive rejection algorithm.

IV. Static FC features and its benefits over activation features for screening biomarkers

Instead of epoch rejections done by the adaptive rejection algorithm, a method to reject datapoints was developed. Spikes were identified by the great amplitude changes (> 0.1 mM·mm) within two datapoints. Moreover, abnormal amplitudes caused by any noises were detected by outlier amplitudes ($\Delta C{\cdot}L > \mu + 3\sigma \ \vee \ \Delta C{\cdot}L < \mu - 3\sigma$; μ and σ are amplitude average and standard deviation of all channels). Datapoints associated with spikes or abnormal amplitudes were rejected; uniform rejections were done for all channels. The remaining datapoints were concatenated according to the BS and (OB) stimulus intervals.

Functionally connected regions are represented by high (Pearson's) correlation coefficients between regions. Static FCs were evaluated in each interval (Figure 5). Stimulus-evoked FC increases were found to be prominent for disordered children in the bilateral intra- and interhemispheric FCs. TD children showed more preserved FCs even during the baseline interval. Even though disordered children experienced the increased right MFG FCs during the stimulus interval, the strength was still weaker compared to that of TD children (two-sample *t*-test, $p < 0.05$, $t_{(47-50)} = 2.34–3.08$).

Both activation and static FC features were optimized using the stepwise-forward method and validated (5-fold) to achieve the highest classification accuracy between TD and disordered children. Static FC features performed better than activation features for training and test subsets (75% vs. 86–90% in average, Table 1). FC-based biomarkers performed better than the previously reported activation-based biomarkers.[29] These results confirmed the benefits of static FC features for screening biomarkers. The discriminative static FC features were found in the bilateral fronto-parietal regions.

V. Distinct dynamic FC characteristics for TD and ADHD children

The dynamic FC analysis commonly performs on the resting-state data;[30,31] the current study is the first work of

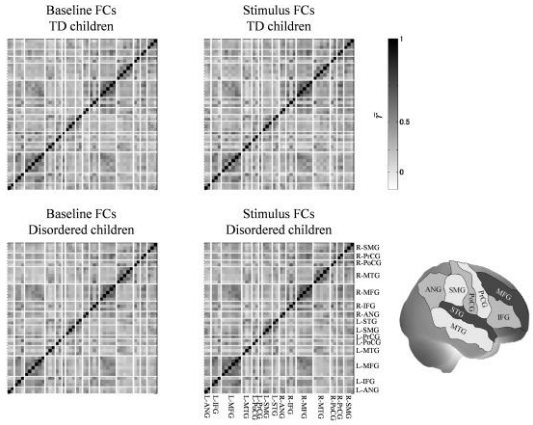

Figure 5. Static FC maps (channel-wise $\bar{r}$) in the baseline and stimulus intervals for TD and disordered children. Channels are categorized following the estimated brain regions (L: left and R: right). From [34], modified with permission.

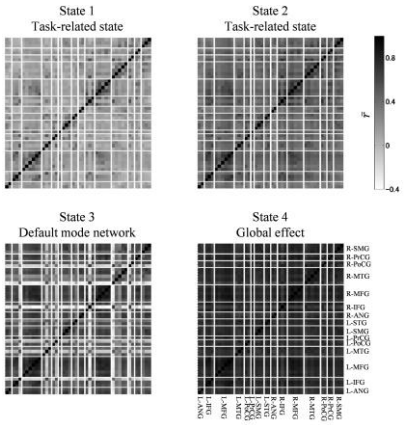

Figure 6. Four connectivity states (channel-wise $\bar{r}$) Channels are categorized following the estimated brain regions (L: left and R: right). From [35], modified with permission.

Table 1. Screening performances

	Activation	Baseline FC	Stimulus FC
Training subsets	74.6±3.4%	86.5±2.5%	89.7±2.6%
Test subsets	74.7±14.9%	85.6±7.9%	90.4±9.6%

the dynamic FC analysis on the task-based fNIRS data. During the GNG task, four connectivity states were found to alternate (Figure 6). Two connectivity states were presumed as the task-related connectivity states due to the strongly observed attentive frontoparietal network. Those connectivity states dominantly occurred (17–67% probability, one-way ANOVA, $p < 10^{-10}$, $\chi^2_{(3,160)} = 51.7$–97.5). The task-irrelevant connectivity states, such as default mode network and global effects were interpreted from the other connectivity states (<17% probability). TD children were found to maintain the task-related connectivity states in both baseline and stimulus intervals, while ADHD children showed decreased occurences of the task-related connectivity states in the transition and stimulus interval (Wilcoxon rank-sum test, $p < 0.05$, $z = -2.76 – -1.96$). Furthemore, the occurrence probability of task-irrelevant connectivity states were heightened for ADHD children (Wilcoxon rank-sum test, $p < 0.05$, $z = 1.96–3.18$).

VI. Conclusion

Three analysis frameworks were established to properly remove noises and analyze brain characteristics (i.e., activation, static and dynamic FCs) from the task-based measurement. The developed adaptive rejection algorithm was promisingly used as a substitute for the laborious visual judgment.[32] The differential diagnostic[33] and screening[34] biomarkers were found by supports of those analysis frameworks. Moreover, the pathophysiological understanding became clearer. ADHD children suffered from impaired FC maintenance and connectivity state recruitment during the task.[35] TD children' attention relatively engaged even in the baseline interval with the lowest cognitive load.

References:

1 Boyle, C. A. *et al. Pediatrics* **127**(6), 1034–1042 (2011).
2 Zablotsky, B. *et al. Pediatrics* **144**(4), e20190811 (2019).
3 Hill, H. A. *et al. Morb Mortal Wkly Rep* **64**(33), 889–896 (2015).
4 Döpfner, M. *et al. Eur Child Adoles Psy* **17** (Suppl 1), 59–70 (2008).
5 Adornetto, C. *et al. Child Adolesc Psychiatry Ment Health* **6**, 40 (2012).
6 Fu, C. H. Y. & Costafreda, S. G. *Can J Psychiatry* **58**(9), 499–508 (2013).
7 Hager, B. M. & Keshavan, M. S. *Curr Behav Neurosci Rep* **2**, 102–111 (2015).
8 Obrig, H. *et al. Int J Psychophysiol* **35**(2–3), 125–142 (2000).
9 Boas, D. A. *et al. NeuroImage* **85**, 1–5 (2014).
10 Ferrari, M. & Quaresima, V. *NeuroImage* **63**(2), 921–935 (2012).
11 Monden, Y. *et al. NeuroImage Clin* **1**(1), 131–140, (2012).
12 Nagashima, M. *et al. Neurophotonics* **1**(2), 025007 (2014).
13 Nagashima, M. *et al. NeuroImage Clin* **6**, 192–201 (2014).
14 Nagashima, M. *et al. Neurophotonics* **1**(1), 015001 (2014).
15 Germon, T. J. *et al. J Clin Monit Comput* **14**(5), 353–360 (1998).
16 Obrig, H. *et al.. NeuroImage* **12**(6), 623–639 (2000).
17 Tachtsidis, I. *et al. Adv Exp Med Biol* **614**, 21–28 (2008).
18 Tong, Y. & Frederick, B. D. *NeuroImage* **53**(2), 553–564 (2010).
19 Scholkmann, F. *et al. Physiol Meas* **31**(5), 649–662 (2010).
20 Brigadoi, S. *et al. NeuroImage* **85**, 181–191 (2014).
21 Maki, A. *et al. Med Phys* **22**(12), 1997–2005 (1995).
22 Niu, H. & He, Y. *The Neuroscientist* **20**(2), 173–188 (2013).
23 Tak, S. & Ye, J. C. *NeuroImage* **85**, 72–91 (2014).
24 Liu, X. & Duyn, J. H. *PNAS* **110**(11), 4392–4397 (2013).
25 Birn, R. M. *et al. NeuroImage* **31**(4), 1536–1548 (2006).
26 Chang, C. *et al. NeuroImage* **68**, 93–104 (2013).
27 Murphy, K. *et al. NeuroImage* **80**, 349–359 (2013).
28 Tokuda, T. *et al. Neuropsychiatry (London)* **8**(3), 917–929 (2018).
29 Ishii-Takahashi, A. *NeuroImage Clin* **4**, 53–63 (2014).
30 Li, Z. *et al. Biomed Opt Express* **6**(7), 2337–2352 (2015).
31 Niu, H. *et al. Neurophotonics* **6**(2), 025010 (2019).
32 Sutoko, S. *et al. Neurophotonics* **5**(4), 045001 (2018).
33 Sutoko, S. *et al. Front Hum Neurosci* **13**, 7 (2019).
34 Sutoko, S. *et al. Neurophotonics* **6**(4), 045013 (2019).
35 Sutoko, S. *et al. Front Hum Neurosci* **14**, 3 (2020).